JACS
JOURNAL OF THE AMERICAN CHEMICAL SOCIETY
Article
pubs.acs.org/JACS

Graphitic Carbon Conformal Coating of Mesoporous TiO_2 Hollow Spheres for High-Performance Lithium Ion Battery Anodes

Hao Liu,[†] Wei Li,[‡] Dengke Shen,[‡] Dongyuan Zhao,*[,‡] and Guoxiu Wang*[,†]

[†]Centre for Clean Energy Technology, School of Mathematics and Physical Sciences, Faculty of Science, University of Technology Sydney, Sydney, New South Wales 2007, Australia

[‡]Department of Chemistry, Laboratory of Advanced Materials, Shanghai Key Lab of Molecular Catalysis and Innovative Materials, iChEM, and State Key Laboratory of Molecular Engineering of Polymers, Fudan University, Shanghai 200433, P. R. China

Supporting Information

ABSTRACT: Rational design and controllable synthesis of TiO_2 based materials with unique microstructure, high reactivity, and excellent electrochemical performance for lithium ion batteries are crucially desired. In this paper, we developed a versatile route to synthesize hollow TiO_2/graphitic carbon (H-TiO_2/GC) spheres with superior electrochemical performance. The as-prepared mesoporous H-TiO_2/GC hollow spheres present a high specific surface area (298 m^2 g^{-1}), a high pore volume (0.31 cm^3 g^{-1}), a large pore size (~5 nm), well-defined hollow structure (monodispersed size of 600 nm and inner diameter of ~400 nm, shell thickness of 100 nm), and small nanocrystals of anatase TiO_2 (~8 nm) conformably encapsulated in ultrathin graphitic carbon layers. As a result, the H-TiO_2/GC hollow spheres achieve excellent electrochemical reactivity and stability as an anode material for lithium ion batteries. A high specific capacity of 137 mAh g^{-1} can be achieved up to 1000 cycles at a current density of 1 A g^{-1} (5 C). We believe that the mesoporous H-TiO_2/GC hollow spheres are expected to be applied as a high-performance electrode material for next generation lithium ion batteries.

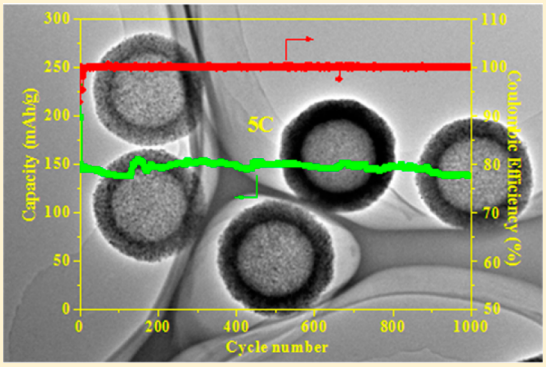

INTRODUCTION

Titanium dioxide (TiO_2) has been extensively investigated in many applications owing to its unique properties, which include abundance, environmental benignancy, safety, and stability. It has been commercialized in many fields of our daily life, such as a white pigment in paint and a UV absorber in sunscreens. Moreover, TiO_2 materials exhibit excellent properties in many advanced applications, including photocatalysts, sensors, drug delivery, and energy storage.[1] Synthetic methods for nanostructured TiO_2 materials from zero to three-dimensional (3D) structure have attracted enormous interest.[2] Substantial research on preparation, characterization, and fundamental understanding has boosted the utilization of TiO_2 nanomaterials with outstanding performance in the past decades.[3]

Rechargeable lithium ion batteries are considered as the most promising energy storage devices for electric vehicles (EVs), owing to their high energy density, compared with other energy storage systems.[4] The central role of building next generation lithium ion batteries is developing electrode materials which can operate at high currents to supply higher powers.[5] Nanostructured materials have attracted great attention in lithium ion batteries because their low dimensions provide shorter pathways and high diffusion dynamics for lithium ion migration.[6] Anatase, rutile, and TiO_2(B) with varying nanostructures have been investigated as anode materials for lithium ion batteries.[7] However, owing to the low conductivity of semiconductive TiO_2 materials, they generally display poor high-rate properties and long-term performance as anode materials for lithium ion batteries. Researchers have tried to combine TiO_2 with highly conductive materials, such as carbon nanotubes (CNTs) and graphene, to boost the electronic conductivity, and hence to improve the electrochemical performance of TiO_2.[8] Nevertheless, in most cases, TiO_2 nanoparticles on the CNT or graphene surface would still suffer from the drastic volume expansion and disintegration during the charge/discharge process. As a result, the electrochemical performances of these anodes would gradually degrade upon cycling. Another effective way to enhance high-rate performances is the carbon coating on TiO_2 nanostructures.[9] However, the electrochemical performance of carbon coating TiO_2 is inferior if the carbon layers do not conformably encapsulate primary tiny TiO_2 nanoparticles and the uncoated areas remain vulnerable with low conductivity.[9a] In addition, the ionic and electronic mobilities in amorphous carbon layers are lower than those of graphitic carbon. Thus, amorphous carbon would prevent lithium ions from diffusion to some extent, and the electrochemical performance is not compatible to graphitic carbon coating. Therefore, conformal coating of ultrathin graphitic carbon on primary tiny active nanoparticles

Received: August 18, 2015
Published: September 28, 2015

DOI: 10.1021/jacs.5b08743
J. Am. Chem. Soc. 2015, 137, 13161−13166

into well-defined nanostructures is greatly desired to achieve excellent electrochemical performance.

Herein, we report a versatile conformal coating strategy to prepare mesoporous hollow TiO_2/graphitic carbon (denoted as H-TiO_2/GC) spheres. In this case, each TiO_2 nanoparticle in the hollow shell is conformably coated by ultrathin graphitic carbon layers (2−3 graphene layers). An ensemble of these hybrid nanoparticles results in a highly conductive and porous network (a specific surface area of 298 m^2 g^{-1}). As a result, the H-TiO_2/GC spheres deliver a high capacity of ∼200 mAh g^{-1} and good initial Coulombic efficiency of about 89.3% at a current density of 0.1 A g^{-1} and, more importantly, shows a superior high-rate performance and long-term life (a retention capacity of 137 mAh g^{-1} up to 1000 cycles at a current density of 1 A g^{-1}).

EXPERIMENTAL SECTION

Synthesis of Materials. The synthesis route of the hollow spherical H-TiO_2/GC composites is schematically illustrated in Scheme 1. First, colloidal SiO_2 nanospheres with a uniform diameter of ∼400 nm were prepared by a well-known Stöber method.[10] Then, mesoporous amorphous TiO_2 shells could homogeneously be deposited onto the SiO_2 nanospheres without using any surfactants via a versatile kinetics-controlled coating method.[11] Typically, the as-prepared SiO_2 nanospheres (0.2 g) were dispersed in ethanol (150 mL). Ammonia solution (0.9 mL, 25 wt %) was added to the suspension, and the mixture was stirred by magnetic bar for 1 h. Then, tetrabutoxide titanate (TBOT, 2.0 mL) was added dropwise over 10 min, and the reaction proceeded at 45 °C for 24 h under continuous stirring. The resultant product was alternately centrifuged and washed with deionized water and ethanol 3 times, respectively. The as-prepared SiO_2@TiO_2 core−shell structured spheres were placed in glucose solution (0.1 M, 15 mL) in an autoclave and hydrothermally treated at 180 °C for 2 h, yielding SiO_2@TiO_2/C spheres. In this step, glucose was decomposed and filled in the interior space of the mesoporous TiO_2 networks, forming TiO_2/C hybrid shells. Then, the obtained spheres were annealed at 800 °C for 5 h with a slow ramping rate (2 °C/min) in argon atmosphere. In this calcination process, the amorphous TiO_2/C shells could be *in situ* converted to crystalline TiO_2/graphitic carbon hybrid structures. After etching by 5% HF solution, the SiO_2 nanospheres could be removed, and H-TiO_2/GC spheres were obtained. after filtration and drying at 50 °C. As a control, the mesoporous TiO_2 hollow spheres (denoted as H-TiO_2) were synthesized by directly sintering SiO_2@TiO_2 core−shell structured spheres at 500 °C in air atmosphere for 5 h and etching with 5% HF.

Scheme 1. Schematic Illustration of the Formation of Conformal Graphitic Carbon Coating of Mesoporous TiO_2 Hollow (Denoted as H-TiO_2/GC) Spheres[a]

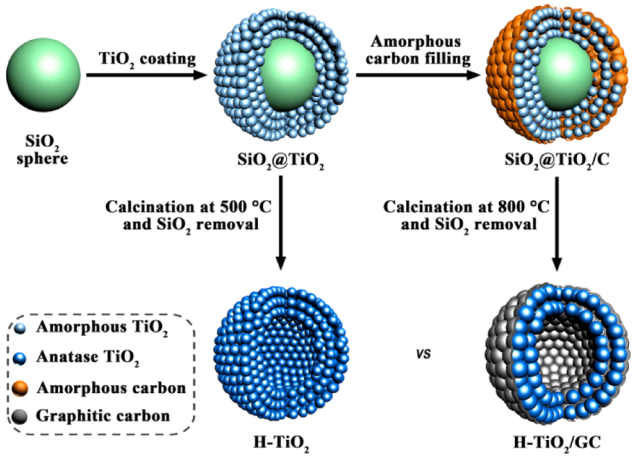

[a]As a control, mesoporous TiO_2 hollow spheres (denoted as H-TiO_2) can be obtained without the carbon coating process.

Characterization. X-ray diffraction (XRD) patterns were obtained from a Bruker D8 diffractometer within 2θ range from 10° to 80°, by using a Cu Kα radiation source (λ = 0.154 06 nm). N_2 adsorption−desorption isotherms were obtained by using a Micromeritics 3Flex analyzer at the testing temperature of 77 K. Brunauer−Emmett−Teller (BET) and Barret−Joyner−Halenda (BJH) analyses were used to determine the surface area, pore volume, and pore size distribution. The BET surface area was calculated using experimental points at a relative pressure of P/P_0 = 0.05−0.25. The pore size distribution was derived from the adsorption branch using the BJH method. The total pore volume was estimated by the nitrogen amount adsorbed at a relative pressure (P/P_0) of 0.995. The morphologies of the samples were obtained from a field-emission scanning electron microscope (FESEM, Zeiss Supra 55VP). The crystalline microstructures of materials were observed by transmission electron microscopy (TEM), high-resolution TEM (HRTEM) analysis, and scanning transmission electron microscopy (STEM, JEOL JEM-ARM200F, at an accelerating voltage of 220 kV).

Cell Assembly and Electrochemical Testing. The anode electrodes were fabricated by mixing the active materials (H-TiO_2/GC hollow spheres) with a binder, poly(vinylidene fluoride) (PVDF), at a weight ratio of 9:1. Traditional carbon additive was excluded in electrodes owing to the existence of graphitic carbon in the H-TiO_2/GC spheres. This technology would reduce the cost of cell fabrication in real applications. The mixture was dispersed in *n*-methyl pyrrolidone (NMP) solvent to form a slurry and then uniformly pasted onto Cu foils with a blade. The electrodes were dried at 120 °C in a vacuum oven for 12 h and subsequently pressed at a pressure of 200 kg cm^{-2}. For comparison, the anatase H-TiO_2 (obtained at 500 °C, the same crystalline structure to that of H-TiO_2/GC obtained at 800 °C) electrodes were prepared by mixing carbon black and PVDF at a weight ratio of 8:1:1, so that it contained the same carbon content as H-TiO_2/GC spheres. CR2032-type coin cells were assembled in a glovebox for electrochemical characterization. A nonaqueous solution of 1 M $LiPF_6$ in a 1:1:1 of ethylene carbonate (EC), diethyl carbonate (DEC), and dimethyl carbonate (DMC) was used as the electrolyte. Li metal disks were used as the counter electrodes for electrochemical testing. The cells were galvanostatically charged and discharged in a current density range of 0.1 A g^{-1} within the voltage range of 1.2−2.5 V. For the high rate testing, the charge/discharge current gradually increased from 0.1 to 0.2, 0.5, 1, 2, 5, and 10 A g^{-1} (equal to 0.5, 1, 2, 5, 10, 20, and 50 C, respectively), then decreased to 1 and 0.1 A g^{-1}, step by step. Cyclic voltammetry (CV) curves were collected by an electrochemistry workstation (CHI660C) at 0.5 mV s^{-1} within a range 0.01−3.0 V. For the electrochemical impedance spectroscopy (EIS) measurements, the excitation voltage applied to the cells was 5 mV. The activation energy measurements were collected between 100 kHz to 100 mHz at different temperatures of between 35 to 55 °C, respectively.

RESULTS AND DISCUSSION

The scanning electron microscopy (SEM) image of the mesoporous hollow spherical H-TiO_2/GC samples shows large-scale monodispersed spheres with a uniform size of about 600 nm (Figure 1a). The high-magnification SEM image (Figure 1b) clearly discloses that the uniform spheres consist of primary nanoparticles with a small size of ∼10 nm. The hollow structure can be confirmed by TEM images (Figure 1c). All hollow spheres show a uniform shell thickness of about 80−90 nm and an inner cavity of ∼400 nm, which is attributed to the removal of the SiO_2 nanosphere templates (Figures S1−S5). The selected area electron diffraction (SAED) pattern (inset in Figure 1c) of the H-TiO_2/GC sample implies the polycrystalline structure. The ring patterns can be indexed with the

DOI: 10.1021/jacs.5b08743
J. Am. Chem. Soc. 2015, 137, 13161−13166

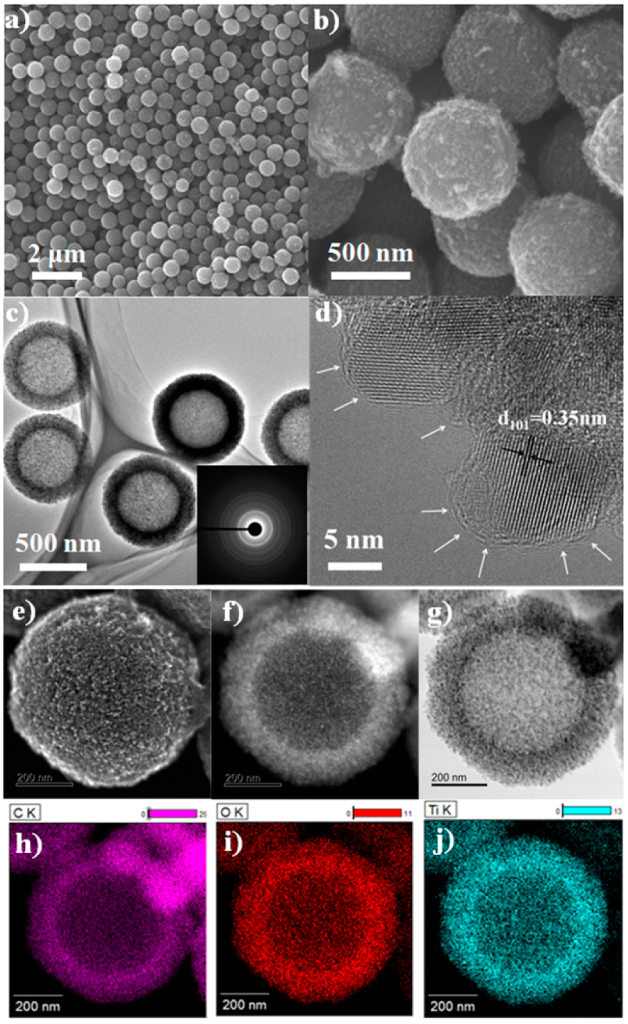

Figure 1. (a, b) SEM and (c) TEM images of the mesoporous H-TiO_2/GC hollow spheres prepared via a versatile conformal coating strategy. Inset in part c is the SAED pattern of the sample H-TiO_2/GC. (d) HRTEM image of the H-TiO_2/GC hollow spheres. (e) Scanning transmission electron microscopy (STEM), (f) high-angle annular dark field (HAADF), and (g) bright field images of a single H-TiO_2/GC sphere. (h–j) EDS mapping of C, O, and Ti elements, implying uniformly elemental distribution in the H-TiO_2/GC sphere.

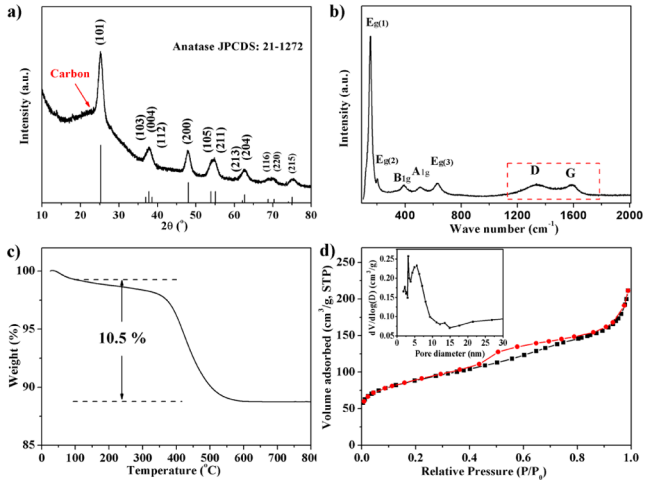

Figure 2. (a) Wide-angle XRD patterns, (b) Raman spectrum, (c) TGA curve, and (d) nitrogen sorption isotherms, and corresponding pore size distribution curve (inset) of the mesoprous H-TiO_2/GC hollow spheres prepared via a versatile conformal coating strategy.

standard anatase phase. The microstructure of the TiO_2 nanoparticles on the shells of H-TiO_2/GC is clearly observed by the high-resolution TEM (HRTEM) image (Figure 2d). The HRTEM image of the H-TiO_2/GC spheres clearly demonstrates that the TiO_2 nanoparticles are well-crystallized with a size of about 10 nm and conformably coated by ultrathin graphitic carbon layer (2–3 graphene layers, as denoted by arrows in Figure 1d). The interplanar distance of the TiO_2 nanoparticles is measured to be ~0.35 nm, which is well-matched with the *d*-spacing of (101) planes of anatase TiO_2. Scanning transmission electron microscopy (STEM) technology was used to investigate the microstructure of a single H-TiO_2/GC sphere (Figure 1e–g). The STEM, high-angle annular dark field (HAADF), and bright field TEM images further confirm a hollow structure of the H-TiO_2/GC spheres with a highly mesoporous shell. The energy dispersed spectrum (EDS) of a single hollow sphere proves the existence of carbon, oxygen, and titanium elements (Figure S7). The corresponding elemental mapping results of the above-mentioned three elements are shown in Figure 1h–j, indicating the homogeneous distribution of C, O, and Ti elements in the shells.

The X-ray diffraction (XRD) pattern of the mesoporous hollow H-TiO_2/GC spheres exhibits well-defined diffraction peaks within the 2θ range from 10° to 80° (Figure 2a), which can be indexed with anatase phase (JPCDS no. 21-1272). An additional broad diffraction peak at the 2θ of ~24° can be found with an overlap by the TiO_2 (101) peak, which can be attributed to the (002) peak of graphitic carbon. On the contrary, this diffraction peak could not be found in H-TiO_2 spheres (Figure S10). The crystal size calculated from the Scherrer equation is about 8 nm, which is consistent with the TEM results. The component of the H-TiO_2/GC spheres was analyzed by Raman microscopy (Figure 2b). The bands at 152, 201, 393, 515, and 642 cm^{-1} correspond to the typical $E_{g(1)}$, $E_{g(2)}$, B_{1g}, A_{1g}, and $E_{g(3)}$ vibrational modes of the Ti–O bonds, respectively.[fb,12] The bands at 1357 and 1580 cm^{-1} are typical D and G lines of graphitic carbon.[13] The value of I_G/I_D is measured to be about 0.53, indicating a relative high degree of graphitic structure.[14]

The carbon content in the H-TiO_2/GC sphere was examined by thermogravimetric analysis (TGA), as shown in Figure 2c. The weight loss below 100 °C can be attributed to the elimination of moisture in the spheres. The H-TiO_2/GC lost its weight between 380 and 530 °C, which can be attributed to the combustion of carbon in the air. The carbon ratio is calculated to be 10.5%. Nitrogen sorption isotherms of the mesoporous hollow H-TiO_2/GC spheres show a type-IV curve (Figure 2d). The specific surface area is calculated to be 298 m^2 g^{-1}, which is higher than that of H-TiO_2 spheres even calcinized at a relatively lower temperature of 500 °C (244 m^2 g^{-1}, Figure S11). The H-TiO_2/GC spheres exhibit a narrow pore size distribution at about 5 nm, and the pore volume is calculated to be a relevant high value of ~0.31 cm^3 g^{-1}.

The key step for the synthesis of the mesoporous hollow TiO_2/graphitic carbon spheres is the amorphous carbon filling in the mesoporous SiO_2@TiO_2 core–shell spheres. Owing to the mesoporous shell structure resulted from well-packed TiO_2 nanoparticles, glucose solution can penetrate into the whole shells and decompose under the confinement, thus leading to a conformal amorphous carbon coating with the internal void

DOI: 10.1021/jacs.5b08743
J. Am. Chem. Soc. 2015, 137, 13161–13166

space during a hydrothermal reaction. When being annealed at 800 °C, graphitic carbon layers can be obtained due to the catalytic effect of TiO_2 nanoparticles, which is similar to the catalytic effect of nanosized catalysts in a previous report.[14] On the other hand, the carbon coating layers can suppress the growth of TiO_2 grains (Figure S4) and confine the phase transformation from anatase to rutile (Figures S9 and S10), which is similar to the silica or carbon protection calcination processes reported previously.[15]

Figure 3a shows the 1st, 2nd, and 100th charge/discharge curves of the mesoporous TiO_2/graphite hollow sphere

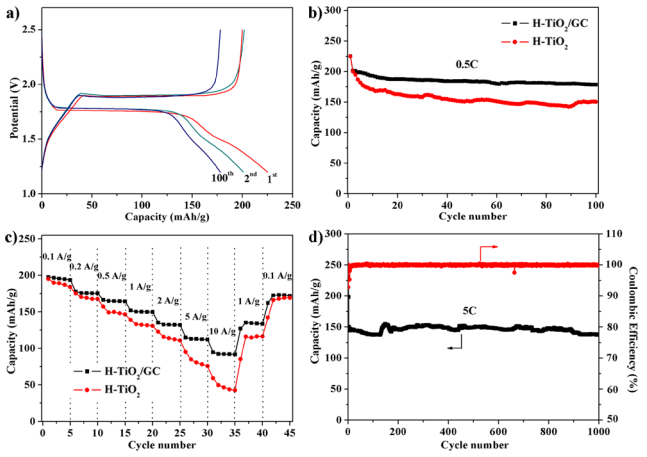

Figure 3. (a) Charge/discharge curves of the mesoporous H-TiO_2/GC hollow spheres at a current density of 0.1 A g^{-1}. (b) Cycling performances of H-TiO_2/GC and H-TiO_2 spheres at a constant current density of 0.1 A g^{-1} (approximate to 0.5 C). (c) Multirate performances of H-TiO_2/GC and H-TiO_2 spheres at different current densities from 0.1 to 10 A g^{-1}, and then returning to 1 and 0.1 A g^{-1}. (d) Long-term performance and Coulombic efficiency of the mesoporous H-TiO_2/GC hollow spheres at a current density of 1 A g^{-1} (5 C) with up to 1000 cycles, implying an outstanding electrochemical retention.

electrodes at a current density of 0.1 A/g within the range 1.2−2.5 V versus Li^+/Li. The plateaus occurred around the potential of 1.5/1.9 V and are ascribed to the insertion/extraction of lithium to anatase TiO_2. The initial charge/discharge capacities of the H-TiO_2/GC hollow spheres are ∼225 and 201 mAh g^{-1}, respectively, demonstrating a good Coulombic efficiency of about 89.3%. In the second cycle, the charge/discharge capacities decrease to 200 and 199 mAh g^{-1}, which are 88% and 99% of their initial capacities. After 100 cycles, the H-TiO_2/GC hollow sphere electrode still delivers a discharge capacity of ∼178 mAh g^{-1}, which is 89% retention of the second cycle. It indicates a slow capacity fading of only 0.11% per cycle. As a control, the electrochemical performance of the H-TiO_2 sphere electrode was also evaluated, since they have properties to those of the H-TiO_2/GC spheres only without the graphitic carbon coating (Table S1). The initial and second discharge capacities of the H-TiO_2 spheres are ∼225 and 200 mAh g^{-1} at a current density of 0.1 A/g, respectively (Figure 3b). However, after 100 cycles, the discharge capacity of the H-TiO_2 sphere electrode is only 150 mAh g^{-1} (75% retention of the second cycle), which is smaller than that of the H-TiO_2/GC hollow sphere electrodes.

The rate capabilities of the H-TiO_2/GC and H-TiO_2 sphere electrodes are then evaluated by charging/discharging at various current densities (Figure 3c). It is clear that the capacity of H-TiO_2 spheres fades rapidly during the high-rate cycling. The capacities of H-TiO_2 are 182, 169, 148, 127, 113, 81, and 42 mAh g^{-1} at the current rates of 0.1, 0.2, 0.5, 1, 2, 5, and 10 A g^{-1}, respectively. In contrast, the H-TiO_2/GC hollow spheres deliver much higher capacities of 191, 177, 164, 151, 131, 114, and 91 mAh g^{-1}, respectively, demonstrating an excellent high-rate performance for the high-power lithium ion battery. Furthermore, when the test currents are regularly returned to low current rates of 1 and 0.1 A g^{-1}, the discharge capacities are recovered to 131 and 173 mAh g^{-1}, which are close to the values in previous measurements. More interestingly, the H-TiO_2/GC hollow sphere electrode can still deliver a high capacity of ∼137 mAh g^{-1} even at a high current rate of 1 A g^{-1} (approximately 5 C) after 1000 cycles, showing only 0.008% fading per cycle (Figure 3d). The initial Coulombic efficiency is about 85.6%, and subsequent Coulombic efficiencies are gradually increased and stably retain near 100%. To our knowledge, the electrochemical property of the mesoporous H-TiO_2/GC hollow spheres is one of the best electrochemical performances (in terms of specific capacity, retention, and Coulombic efficiency) among the TiO_2 based electrode materials (Table S2).[7a−f,j,k,9b]

Cyclic voltammetry (CV) curves of the H-TiO_2 and H-TiO_2/GC spheres display cathodic/anodic peaks located at around 1.70 and 2.05 V (versus Li^+/Li) (Figure 4a), which are

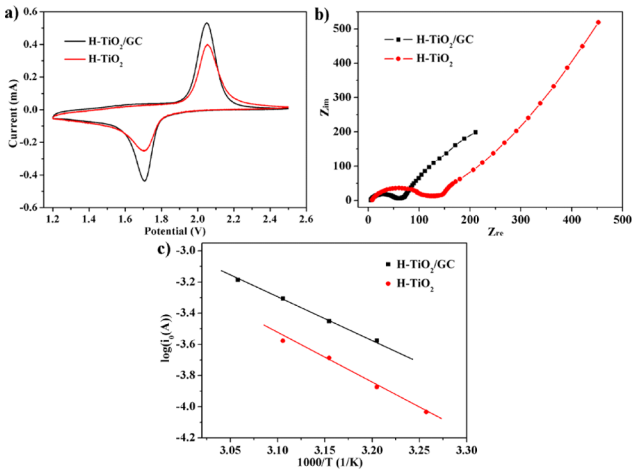

Figure 4. (a) Cyclic voltammetry (CV) curves of H-TiO_2/GC and H-TiO_2 sphere electrodes with a scanning rate of 0.5 mV/s. (b) Nyquist plots of H-TiO_2/GC and H-TiO_2 spheres at room temperature. (c) Arrhenius plots of log i_0 versus $1/T$ for fresh electrodes of H-TiO_2/GC and H-TiO_2 spheres collected at 2 V at different temperatures from 35 to 55 °C.

associated with lithium insertion/extraction in the anatase lattice. The higher intensity of the redox peaks of the H-TiO_2/GC composites than H-TiO_2 spheres can be attributed to the higher electrochemical activity. In addition, the H-TiO_2/GC hollow sphere electrode shows a lower polarization in initial cycle (Figure S12) due to enhanced electronic conductivity by graphitic carbon coating. The H-TiO_2/GC sphere electrode also indicates a decreased potential separation between reduction and oxidation peaks (Figure S12c), which is associated with the higher reversibility. Both Nyquist plots of H-TiO_2/GC and H-TiO_2 spheres present a depressed semicircle in the moderate frequency region and a straight line in the low-frequency region, which are relevant to a charge transfer process and a Warburg diffusion process, respectively

DOI: 10.1021/jacs.5b08743
J. Am. Chem. Soc. 2015, 137, 13161−13166

(Figure 4b). In a high-frequency region, the H-TiO_2/GC hollow spheres show a lower value across the real resistance (R_{re}) axis, demonstrating a lower overall resistance than that of the H-TiO_2 sphere electrode (4.6 vs 7.1 Ohms, Figure S13). On the other hand, the H-TiO_2/GC spheres exhibit a lower charge transfer resistance (R_{ct}, 56 Ohms) than that of H-TiO_2 (119 Ohms), as shown in the moderate frequency region, which can lead to faster lithium ion diffusion in the solid state of the electrode. Figure 4c shows Arrhenius plots of log i_0 versus $1/T$ for the H-TiO_2/GC and H-TiO_2 spheres, which are derived from EIS results as shown in Figure S14. The activation energies are 58.97 and 51.42 kJ mol^{-1} for the H-TiO_2 and H-TiO_2/GC spheres, respectively, as calculated from the Arrhenius plots, indicating higher lithium ion diffusion kinetics in the H-TiO_2/GC spheres.

SEM and TEM images (Figure 5a–c) of the H-TiO_2/GC sphere electrode after 100 cycles show well-defined hollow

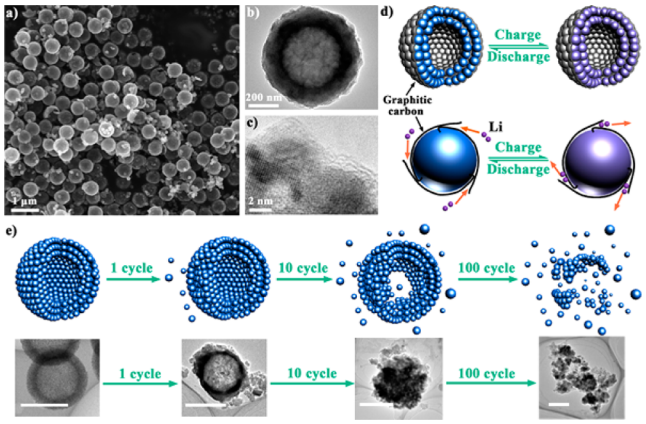

Figure 5. (a) SEM, (b) TEM, and (c) HRTEM images of the mesoporous H-TiO_2/GC hollow spheres after 100 cycles. (d) Schematic illustrations showing that the graphitic carbon conformal coating layers can buffer the volume expansion of TiO_2 nanoparticles, thus maintaining the rigid structure of H-TiO_2/GC spheres with cycling. (e) Schematic illustrations showing the structure evolution of H-TiO_2 spheres upon cycling and the corresponding TEM images. All scale bars are 500 nm in the TEM images in part e.

spherical structures, and the crystalline TiO_2 nanoparticles are still conformably encapsulated by graphitic carbon layers, clearly indicating that the H-TiO_2/GC hollow spheres are stable to withstand expansion/shrinkage during lithium ion intercalation/deintercalation. Although the thickness of the shells slightly expanded during the lithium ion insertion/extraction, graphitic carbon layer could buffer the volume change of TiO_2 crystals and thus retain the hollow structure well (Figure 5d). For the H-TiO_2 spheres without carbon coating, the TiO_2 shells suffer the expansion force without any protection to retain the integrity, and TiO_2 nanoparticles would peel from the sphere. The schematic illustrations of the H-TiO_2 sphere structure evolution upon cycling are given, combined with corresponding TEM images (Figure 5e). It is clear that the structure of the H-TiO_2 spheres gradually collapsed with the cycling and completely lost its original spherical shape after long-term testing.

The excellent electrochemical performance of our mesoporous H-TiO_2/GC hollow spheres as an anode for lithium ion battery can be attributed to their unique features. First, it shows a high specific surface area (298 m^2 g^{-1}), a high pore volume (0.31 cm^3 g^{-1}), a large pore size (~5 nm), and a robust hollow structure, which can provide a large amount of active sites (electrode/electrolyte interfaces) for lithium ion diffusion and access. Second, the small TiO_2 nanocrystals (~8 nm) confined by graphitic carbon layers provide short lithium diffusion pathways. As a result, the diffusion dynamics of lithium ions can be greatly enhanced. Third, the graphitic carbon layers can greatly enhance the electronic conductivity of the TiO_2 hollow shells, which leads to a higher electrochemical reactivity and reversibility. Fourth, the graphitized carbon layer can depress the wrapped TiO_2 nanocrystals from volume change. The carbon networks can buffer the expansion/shrinkage and maintain the porous shell structure. The robustness of the hollow sphere H-TiO_2/GC promotes the electrochemical property and achieves enhanced long-term and high-rate performances. In contrast, the H-TiO_2 spheres without carbon coating show a low reactivity and poor structural stability. During a long-term charge/discharge, TiO_2 nanoparticles would exfoliate from the shell, and the hollow structure eventually collapses.

CONCLUSION

In summary, we developed a versatile conformal coating strategy to prepare mesoporous TiO_2/graphitic carbon hollow spheres. The H-TiO_2/GC spheres present a high specific surface area (~298 m^2 g^{-1}), a high pore volume (~0.31 cm^3 g^{-1}), a large pore size (~5 nm), a well-defined hollow structure, and small anatase TiO_2 nanocrystals (~8 nm) conformably encapsulated in ultrathin graphitic carbon layers. When being applied as an anode material, the H-TiO_2/GC sphere electrode can achieve a high capacity of ~178 mAh g^{-1} at a current density of 100 mA g^{-1} after 100 cycles, which is a dramatic improvement compared with H-TiO_2 hollow spheres electrode (150 mAh g^{-1}). More importantly, the H-TiO_2/GC spheres exhibit a superior high-rate performance and deliver a capacity of 137 mAh g^{-1} up to 1000 cycles at a current density of 1 A g^{-1} (~5 C). These results indicate that H-TiO_2/GC is expected to be applied as next generation high-performance electrode materials. This work would be instructive for the enhancement of low-conductive nanostructured materials for lithium ion batteries.

ASSOCIATED CONTENT

Supporting Information

The Supporting Information is available free of charge on the ACS Publications website at DOI: 10.1021/jacs.5b08743.

Microscopic investigations of materials, XRD patterns of materials obtained from different temperatures, nitrogen sorption of H-TiO_2, and physicochemical properties of H-TiO_2 and H-TiO_2/GC (PDF)

AUTHOR INFORMATION

Corresponding Authors

*dyzhao@fudan.edu.cn
*Guoxiu.Wang@uts.edu.au

Author Contributions

H.L. and W.L. contributed equally.

Notes

The authors declare no competing financial interest.

DOI: 10.1021/jacs.5b08743
J. Am. Chem. Soc. 2015, 137, 13161–13166

■ ACKNOWLEDGMENTS

This work was financially supported by the State Key 973 Program of PRC (2013CB934104), the NSF of China (21210004), Shanghai Science Foundation Project (14JC1400700), Australian Research Council (ARC) through Projects of FT110100800 and DE140100619. H.L. would like to acknowledge the support of Chancellor's Post Doctoral Fellowship (CPDF) and International Researcher Development (IRD) program from UTS. The authors acknowledge TEM support from Dr. David Mitchell, using JEOL JEM-ARM200F within the UoW Electron Microscopy Centre (LE120100104).

■ REFERENCES

(1) (a) Fujishima, A.; Honda, K. *Nature* **1972**, *238*, 37. (b) Chen, X. B.; Liu, L.; Yu, P. Y.; Mao, S. S. *Science* **2011**, *331*, 746. (c) Dahl, M.; Liu, Y. D.; Yin, Y. D. *Chem. Rev.* **2014**, *114*, 9853. (d) Rajh, T.; Dimitrijevic, N. M.; Bissonnette, M.; Koritarov, T.; Konda, V. *Chem. Rev.* **2014**, *114*, 10177. (e) Li, W.; Wu, Z. X.; Wang, J. X.; Elzatahry, A. A.; Zhao, D. Y. *Chem. Mater.* **2014**, *26*, 287. (f) Kapilashrami, M.; Zhang, Y. F.; Liu, Y. S.; Hagfeldt, A.; Guo, J. H. *Chem. Rev.* **2014**, *114*, 9662. (g) Wang, Y. Q.; gu, L.; Guo, Y. G.; Li, H.; He, X. Q.; Tsukimoto, S.; Ikuhara, Y.; Wan, L. J. *J. Am. Chem. Soc.* **2012**, *134*, 7874. (h) Liu, B.; Chen, H. M.; Liu, C.; Andrews, S. C.; Hahn, C.; Yang, P. D. *J. Am. Chem. Soc.* **2013**, *135*, 9995.

(2) (a) Sang, L. X.; Zhao, Y. X.; Burda, C. *Chem. Rev.* **2014**, *114*, 9283. (b) Lee, K.; Mazare, A.; Schmuki, P. *Chem. Rev.* **2014**, *114*, 9385. (c) Wang, X. D.; Li, Z. D.; Shi, J.; Yu, Y. H. *Chem. Rev.* **2014**, *114*, 9346. (d) Wang, Z. L.; Sasaki, T. *Chem. Rev.* **2014**, *114*, 9455. (e) Fattakhova-Rohlfing, D.; Zaleska, A.; Bein, T. *Chem. Rev.* **2014**, *114*, 9487.

(3) (a) Yang, H. G.; Sun, C. H.; Qiao, S. Z.; Zou, J.; Liu, G.; Smith, S. C.; Cheng, H. M.; Lu, G. Q. *Nature* **2008**, *453*, 638. (b) Crossland, E. J. W.; Noel, N.; Sivaram, V.; Leijtens, T.; Alexander-Webber, J. A.; Snaith, H. J. *Nature* **2013**, *495*, 215. (c) Setvin, M.; Aschauer, U.; Scheiber, P.; Li, Y. F.; Hou, W. Y.; Schmid, M.; Selloni, A.; Diebold, U. *Science* **2013**, *341*, 988. (d) Satoh, N.; Nakashima, T.; Kamikura, K.; Yamamoto, K. *Nat. Nanotechnol.* **2008**, *3*, 106. (e) Tao, J. G.; Luttrell, T.; Batzill, M. *Nat. Chem.* **2011**, *3*, 296. (f) Hochbaum, A. I.; Yang, P. D. *Chem. Rev.* **2010**, *110*, 527.

(4) Tarascon, J. M.; Armand, M. *Nature* **2001**, *414*, 359.

(5) Bruce, P. G.; Scrosati, B.; Tarascon, J. M. *Angew. Chem., Int. Ed.* **2008**, *47*, 2930.

(6) (a) Kang, B.; Ceder, G. *Nature* **2009**, *458*, 190. (b) Kang, K. S.; Meng, Y. S.; Breger, J.; Grey, C. P.; Ceder, G. *Science* **2006**, *311*, 977.

(7) (a) Zhang, G. Q.; Wu, H. B.; Song, T.; Paik, U.; Lou, X. W. *Angew. Chem., Int. Ed.* **2014**, *53*, 12590. (b) Ye, J. F.; Liu, W.; Cai, J. G.; Chen, S.; Zhao, X. W.; Zhou, H. H.; Qi, L. M. *J. Am. Chem. Soc.* **2011**, *133*, 933. (c) Wang, Z. Y.; Lou, X. W. *Adv. Mater.* **2012**, *24*, 4124. (d) Sun, Z. Q.; Kim, J. H.; Zhao, Y.; Bijarbooneh, F.; Malgras, V.; Lee, Y.; Kang, Y. M.; Dou, S. X. *J. Am. Chem. Soc.* **2011**, *133*, 19314. (e) Chen, J. S.; Tan, Y. L.; Li, C. M.; Cheah, Y. L.; Luan, D. Y.; Madhavi, S.; Boey, F. Y. C.; Archer, L. A.; Lou, X. W. *J. Am. Chem. Soc.* **2010**, *132*, 6124. (f) Hu, Y. S.; Kienle, L.; Guo, Y. G.; Maier, J. *Adv. Mater.* **2006**, *18*, 1421. (g) Armstrong, G.; Armstrong, A. R.; Bruce, P. G.; Reale, P.; Scrosati, B. *Adv. Mater.* **2006**, *18*, 2597. (h) Tang, Y. X.; Zhang, Y. Y.; Deng, J. Y.; Qi, D. P.; Leow, W. R.; Wei, J. Q.; Yin, S. Y.; Dong, Z. L.; Yazami, R.; Chen, Z.; Chen, X. D. *Angew. Chem., Int. Ed.* **2014**, *53*, 13488. (i) Tang, Y. X.; Zhang, Y. Y.; Deng, J. Y.; Wei, J. Q.; Tam, H. L.; Chandran, B. K.; Dong, Z. L.; Chen, Z.; Chen, X. D. *Adv. Mater.* **2014**, *26*, 6111. (j) Wang, D. H.; Choi, D.; Li, J.; Yang, Z. G.; Nie, Z. M.; Kou, R.; Hu, D. H.; Wang, C. M.; Saraf, L. V.; Zhang, J. G.; Aksay, I. A.; Liu, J. *ACS Nano* **2009**, *3*, 907. (k) Ren, H.; Yu, R. B.; Wang, J. Y.; Jin, Q.; Yang, M.; Mao, D.; Kisailus, D.; Zhao, H. J.; Wang, D. *Nano Lett.* **2014**, *14*, 6679. (l) Wang, W. S.; Sa, Q.; Chen, J. H.; Wang, Y.; Jung, H.; Yin, Y. D. *ACS Appl. Mater. Interfaces* **2013**, *5*, 6478.

(8) (a) Chen, Z.; Zhang, D. Q.; Wang, X. L.; Jia, X. L.; Wei, F.; Li, H. X.; Lu, Y. F. *Adv. Mater.* **2012**, *24*, 2030. (b) Mo, R. W.; Lei, Z. Y.; Sun, K. N.; Rooney, D. *Adv. Mater.* **2014**, *26*, 2084. (c) Li, W.; Wang, F.; Feng, S. S.; Wang, J. X.; Sun, Z. K.; Li, B.; Li, Y. H.; Yang, J. P.; Elzatahry, A. A.; Xia, Y. Y.; Zhao, D. Y. *J. Am. Chem. Soc.* **2013**, *135*, 18300. (d) Li, W.; Wang, F.; Liu, Y. P.; Wang, J. X.; Yang, J. P.; Zhang, L. J.; Elzatahry, A. A.; Al-Dahyan, D.; Xia, Y. Y.; Zhao, D. Y. *Nano Lett.* **2015**, *15*, 2186. (e) Qiu, B. C.; Xing, M. Y.; Zhang, J. L. *J. Am. Chem. Soc.* **2014**, *136*, 5852. (f) Cao, F. F.; Guo, Y. G.; Wan, L. J. *Energy Environ. Sci.* **2011**, *4*, 1634.

(9) (a) Fu, L. J.; Liu, H.; Zhang, H. P.; Li, C.; Zhang, T.; Wu, Y. P.; Holze, R.; Wu, H. Q. *Electrochem. Commun.* **2006**, *8*, 1. (b) Xia, T.; Zhang, W.; Wang, Z. H.; Zhang, Y. L.; Song, X. Y.; Murowchick, J.; Battaglia, V.; Liu, G.; Chen, X. B. *Nano Energy* **2014**, *6*, 109.

(10) Stöber, W.; Fink, A. *J. Colloid Interface Sci.* **1968**, *26*, 62.

(11) Li, W.; Yang, J. P.; Wu, Z. X.; Wang, J. X.; Li, B.; Feng, S. S.; Deng, Y. H.; Zhang, F.; Zhao, D. Y. *J. Am. Chem. Soc.* **2012**, *134*, 11864.

(12) (a) Ohsaka, T.; Izumi, F.; Fujiki, Y. *J. Raman Spectrosc.* **1978**, *7*, 321. (b) Chen, X. B.; Mao, S. S. *Chem. Rev.* **2007**, *107*, 2891.

(13) Ferrari, C.; Robertson, J. *Phys. Rev. B: Condens. Matter Mater. Phys.* **2000**, *61*, 14095.

(14) Lee, K. T.; Ji, X. L.; Rault, M.; Nazar, L. F. *Angew. Chem., Int. Ed.* **2009**, *48*, 5661.

(15) (a) Zhang, J.; Xu, Q.; Feng, Z. C.; Li, M. J.; Li, C. *Angew. Chem., Int. Ed.* **2008**, *47*, 1766. (b) Joo, J. B.; Zhang, Q.; Lee, I.; Dahl, M.; Zaera, F.; Yin, Y. D. *Adv. Funct. Mater.* **2012**, *22*, 166. (c) Liu, H. Y.; Joo, J. B.; Dahl, M.; Zeng, Z. Z.; Yin, Y. D. *Energy Environ. Sci.* **2015**, *8*, 286.

DOI: 10.1021/jacs.5b08743
J. Am. Chem. Soc. 2015, 137, 13161−13166